Journal of Power Sources 273 (2015) 981–989

Contents lists available at ScienceDirect

Journal of Power Sources

journal homepage: www.elsevier.com/locate/jpowsour

Non-precious metal nanoparticles supported on nitrogen-doped graphene as a promising catalyst for oxygen reduction reaction: Synthesis, characterization and electrocatalytic performance

Hosna Ghanbarlou [a, b], Soosan Rowshanzamir [a, b, *], Bagher Kazeminasab [c], Mohammad Javad Parnian [a, b]

[a] School of Chemical Engineering, Iran University of Science and Technology, Tehran, 16846-13114, Iran
[b] Fuel Cell Laboratory, Green Research Center, Iran University of Science and Technology, Tehran, Iran
[c] Department of Energy Engineering, Science and Research Branch, Islamic Azad University, Tehran, Iran

HIGHLIGHTS

- Nitrogen-doped graphene (NG) were synthesized through simple solvothermal reaction.
- Fe, Co and Fe–Co nanoparticles were precipitated on NG (M/NG).
- Co/NG exhibited enhanced ORR activity compared to other M/NG catalysts.
- The performance of catalysts was related to uniform distribution of metal particles.

GRAPHICAL ABSTRACT

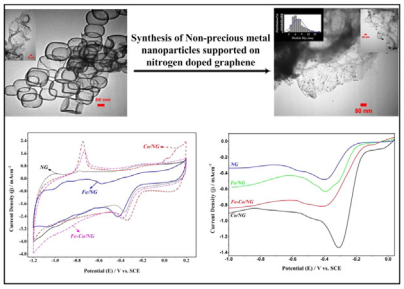

ARTICLE INFO

Article history:
Received 10 July 2014
Received in revised form
19 August 2014
Accepted 1 October 2014
Available online 7 October 2014

Keywords:
Nitrogen-doped graphene
Solvothermal process
Oxygen reduction reaction
Fe, Co and Fe–Co nanoparticles
Electrochemical characterization

ABSTRACT

Nitrogen-doped graphene (NG) based non-precious metal catalysts is used as a catalyst for oxygen reduction reaction (ORR). Nanoflower-like NG with designed nitrogen types is directly synthesized using a low temperature solvothermal process and then Fe, Co and Fe–Co nanoparticles are precipitated onto the NG using a modified polyol method. The morphology of the NG is studied using scanning electron microscopy, transmission electron microscopy and X-ray photoelectron spectroscopy. The synthesized M/NG (M = Fe, Co, Fe–Co) electrocatalysts are characterized using transmission electron microscopy, X-ray diffraction and energy-dispersive X-ray spectroscopy. Electrochemical characterizations reveal that NG acts as a catalyst for ORR in an alkaline solution. The electrocatalytic properties of NG and M/NG catalysts are investigated for ORR in 0.1 M KOH. Cyclic voltammetry, linear sweep voltammetry and electrochemical impedance spectroscopy are used to measure electrocatalytic activity. M/NG catalysts exhibit higher electrocatalytic activity than NG and the highest activity is observed for the Co/NG electrode. Chronoamperometric results demonstrate that the Co/NG catalyst is more stable than commercial Pt/C for ORR in an alkaline solution.

1. Introduction

Development of efficient electrocatalysts for oxygen reduction reaction (ORR) is one of the most important issues for optimizing the performance of fuel cells and metal-air batteries [1,2]. Carbon-

* Corresponding author. Iran University of Science and Technology, P.O. Box: 16846-13114, Tehran, Iran. Tel./fax: +98 2177491242.
E-mail address: rowshanzamir@iust.ac.ir (S. Rowshanzamir).

http://dx.doi.org/10.1016/j.jpowsour.2014.10.001
0378-7753/

supported platinum-based nanomaterials have been regarded as the best electrocatalysts for ORR in these electrochemical energy devices [3]. The cost of Pt catalyst, which is a limited natural resource, will gradually increase over time. Pt-based electrocatalysts also have shown low durability. In addition, during fuel cell operation, platinum nanoparticles usually agglomerate, detach from the carbon support, and can suffer CO poisoning [4]. Accordingly, there is strong motivation to replace platinum with low cost materials, such as platinum binary and ternary alloys [5,6] and transition metal chelates [7]. Much effort has also been devoted to the durability of the support materials [8,9].

Recently, N-doped carbon materials such as vertically aligned N-doped carbon nanotubes [10], nitrogen doped carbon nanocapsules [11], nitrogen-containing porous carbons [12], and nitrogen-doped graphene (NG) [13,14] have been considered as alternative electrocatalysts for ORR. Some of these nitrogen-containing nanocomposites have shown enhanced activity for ORR that is comparable to that of commercial platinum catalyst under alkaline conditions [15–17].

It has been demonstrated that nitrogen-doped carbon supports can increase the durability and activity of catalysts for ORR [18,19]. The strong basicity of N-doped carbon facilitates O_2 adsorption and decomposition of peroxide species that consequently lead to increased ORR electrocatalytic activity [20–22]. Carbon atoms around the nitrogen act as active sites. Nitrogen atoms in the matrix of the carbon withdraw electrons from adjacent carbon atoms because of the higher electronegativity of nitrogen and the resultant positive carbon atoms facilitate activation of ORR [23]. These active sites can also act as anchoring sites for metal nanoparticle deposition [24–26].

Of the nitrogen-containing carbon nanomaterials, NG has received considerable attention because of its strong ability for catalyzing ORR in alkaline media [17,27]. Graphene is a new 2-dimensional carbon material that has intriguing properties, such as high surface area, high electrical conductivity, thermal stability, great electron mobility and a unique graphitic basal plane that guarantees durability. Another important property of graphene is adsorption; the planar structure of graphene makes it a suitable substance for metal nanoparticle deposition and demonstrates its potential as a supporting material for catalyst particles [28].

Pure graphene is actually a highly-graphitized carbon support with a unique graphitized basal plane with fewer active sites for highly graphitized carbon support, making metal nanoparticle deposition difficult. The electrocatalytic performance of graphene can be improved by doping it with heteroatoms such as nitrogen [29]. NG has more structural defects that lead to more uniform dispersion of metal nanoparticles compared to pristine graphene [18,19].

When a nitrogen atom is doped into graphene, it usually has three common bonding configurations within the carbon lattice; the quaternary N (or graphitic N), pyridinic N, and pyrrolic N. Oxides of pyridinic N have also been observed. Most methods for NG synthesis that use different precursors as the carbon and nitrogen sources result in uncontrollable N-doping and produce mixtures of all nitrogen configurations in the resultant NG [14,30,31]. Recent studies have shown that the graphitic and pyridinic nitrogen content in graphene sheets increase ORR activity in a system [32–34]. Pure graphitic and pure pyridinic NG have previously been synthesized [35,36]; however, it has been shown that pyridinic nitrogen alone can not induce effective ORR activity [35]. This means it is important to develop an appropriate synthetic methodology that provides a mixture of pyridinic and graphitic nitrogen in the doped forms of nitrogen in the graphene matrix.

Carbon-supported transition metal/nitrogen (M–N–C, M = Fe, Co, Ni,…) materials have been investigated as promising cathode catalysts for fuel cells. Studies have shown that they produce high electrocatalytic activity for ORR in both acidic and alkaline media [37–41]. Of the transitional metals, iron and cobalt have been found to promote catalysis of ORR in M–N–C catalysts [37,42]. In some cases, the activity of these catalysts was even higher than that of commercial Pt/C, indicating that these electrocatalysts induce an ORR from the desirable 4-electron pathway rather than the 2-electron process [40,41].

The exact nature of the electrocatalytic sites for ORR in these catalysts is still under debate [40,41]. It has been proposed that M–N–C sites can act as electrocatalytic centers for ORR and that metal ions facilitate incorporation of nitrogen into graphene sheets [41,43]. Liu et al. [32] stated that transition metals are not active sites for ORR, but transition metal can facilitate stable doping of nitrogen functional groups into the carbon matrix and increase ORR activity.

Wu et al. [42] studied the role of metal loadings on oxygen reduction activity of binary Fe–Co–N–C catalyst. They found that varying the ratios of Co to Fe and the total metal loading during synthesis led to markedly different activity for oxygen reduction. They believed that the exclusive electrocatalytic properties of Co contribute to the formation of onion-like carbon structures in the binary catalysts.

The modified polyol reduction approach has been shown to be a powerful method for the synthesis of highly-dispersed and optimum particle-sized metal nanoparticles over the surface of the carbon supporting materials. Previous studies have found that the catalysis of the cathodic fuel cell reaction with catalysts synthesized by polyol method is superior compared to those synthesized by conventional sodium borohydride reduction method [44,45] Vinayan et al. [46] synthesized triangular shaped palladium nanoparticles decorated nitrogen doped graphene using the polyol reduction process. They claimed that kinetic control of the growth of the nanoparticles and nitrogen doping of the supporting material formed highly dispersed anisotropic nanoparticles over the graphene support.

In the present work, Fe, Co and Fe–Co nanoparticles were precipitated on nitrogen doped graphene using a modified polyol method. Pentachloropyridine was used as the carbon and nitrogen source for preparation of the NG. The electrochemical performance of the synthesized catalysts, including activity and durability for ORR in alkaline media, was investigated using various electrochemical tests.

2. Experimental

2.1. Synthesis of nitrogen-doped graphene

NG was prepared using a one-pot solvothermal reaction of pentachloropyridine (C_5Cl_5N; Merck) with metallic potassium (K; Sigma Aldrich). The reaction of 1 g pentachloropyridine and K was carried out at 160 °C for 10 h in a stainless steel autoclave reactor (Fig. 1). The product was washed sequentially with acetone, absolute ethanol, and deionized water and dried in a vacuum oven at 80 °C for 4 h [9].

2.2. Synthesis of M/NG (M = Fe, Co, Fe–Co)

In a typical approach, 20 mg NG was dispersed in a mixture of ethylene glycol ($C_2H_6O_2$; Merck) and deionized water by sonication for 1 h. The calculated amounts of transitional metal salts, iron nitrate ($Fe(NO_3)_2 \cdot 6H_2O$; Merck) and cobalt nitrate ($Co(NO_3)_3 \cdot 9H_2O$; Merck) solutions with different percentages of Co:Fe to support material (0:40, 20:20, 40:0) were added to the suspension drop wise and stirred for 1 h. For synthesis of 40 wt.% Fe/NG,

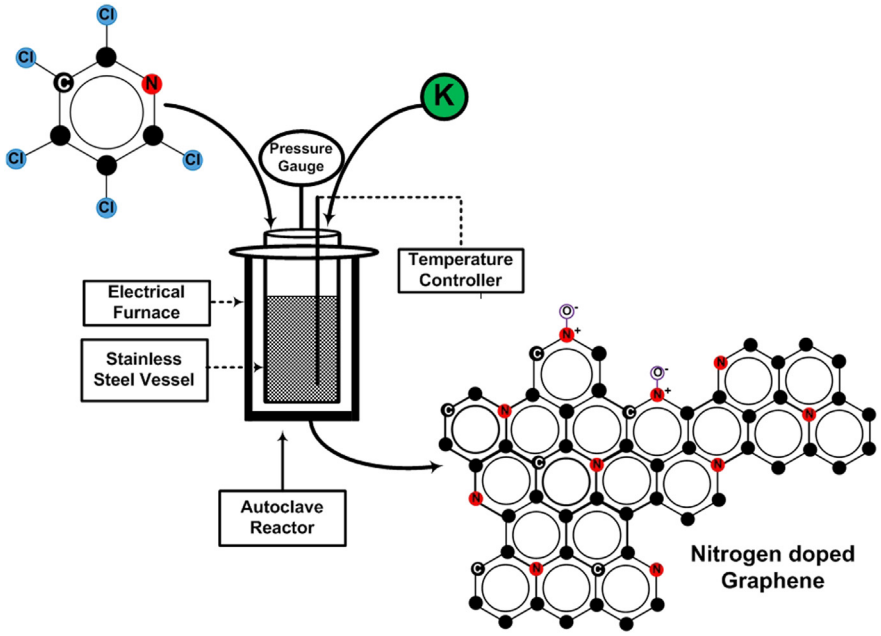

Fig. 1. Schematic illustration of the preparation of nitrogen doped graphene by solvothermal method in autoclave reactor.

57.8 mg iron nitrate and for 40 wt.% Co/NG, 39.5 mg cobalt nitrate were added to suspension solution. The pH of the solution was adjusted to 7 by adding 2.5 M sodium hydroxide (NaOH; Merck) and the solution was heat treated at 60–70 °C for 1 h. In this process, ethylene glycol acts as a reducing, stabilizing and dispersing agent. The solution was centrifuged and washed 3–4 times with deionized water and dried at 70 °C for 8 h in a vacuum oven. The prepared samples were denoted as Fe/NG, Fe–Co/NG and Co/NG. The amount of metal detected by ICP for all samples after precipitation process was very close to the expected values. ICP-MS measurements confirm the content of metals by weight in the Fe–Co/NG sample to be 20 wt.% Fe and 20 wt.% Co with respect to support material and for Fe/NG and Co/NG, the metal content of the samples was identified 40 wt.% with respect to support material.

2.3. Physical characterizations

2.3.1. Scanning electron microscopy

The morphology of the NG samples was obtained using scanning electron microscopy (SEM, Hitachi S-4160) operated at an accelerating voltage of 20 kV.

2.3.2. Transmission electron microscopy

The nanostructure of the materials and distribution of nanoparticles supported on NG were studied using transmission electron microscopy (TEM; ZEISS 900) with an accelerating voltage of 50–80 kV.

2.3.3. X-ray photoelectron spectroscopy

X-ray photoelectron spectroscopy (XPS) data were recorded using an 8025-BesTec twin anode XR3E2 X-ray source system with monochromatic Alkα radiation.

2.3.4. Energy dispersive X-ray

The energy dispersive X-ray (EDX) detector (Horiba XGT-7200) was used for elemental analysis of the catalysts.

2.3.5. Inductively coupled plasma mass spectrometry

The mass contents of Fe and Co in different samples were determined by inductively coupled plasma mass spectrometry (ICP-MS) measurements using a PerkinElmer inductively coupled plasma mass spectrometer (ICP-MS).

2.3.6. X-ray diffraction

X-ray powder diffraction (XRD) was carried out using a Philips PW1800 diffractometer operated at 40 kV and 30 mA using a Cukα radiation source. The cobalt and iron phases were detected by comparing the diffraction patterns with those of standard powder XRD compiled by the Joint Committee on Powder Diffraction Standards. Average cobalt and iron crystallites sizes were calculated using Scherrer's Equation (1) and their most intense peaks:

$$d = \frac{0.89\lambda}{B\mathrm{Cos}\theta} \times \frac{180^{\circ}}{\pi} \quad (1)$$

where d is the mean crystallite size; λ is the X-ray wave length (1.54056 Å); and B is the full width half maximum of the cobalt and iron diffraction peaks.

2.4. Electrochemical measurements

Electrochemical measurements were carried out at room temperature in a conventional three-electrode cell connected to an electrochemical analyzer. Glassy carbon coated with catalyst ink was used as the working electrode. A saturated calomel electrode and a Pt plate were used as reference and counter electrodes, respectively. All potentials were relative to the saturated calomel electrode (SCE). Prior to surface coating, the glassy carbon electrode (GCE) was sequentially polished and then washed with deionized water for a few minutes.

For electrode preparation, 1 mg of total electrocatalyst was dispersed in a 1 mL mixture of 5 wt.% nafion solution and deionized water (volume ratio = 1:9) by sonication. Catalyst dispersion (6 μl) was transferred onto a GCE (2 mm in diameter, 0.031415 cm^2 geometric area) and dried at 80 °C for 15 min. ORR activity can be evaluated by cyclic voltammetry (CV) and linear sweep

voltammetry (LSV). With CV, ORR was measured in oxygen-saturated 0.1 M KOH solution at 25 °C with the scan rate of 100 mV s^{-1} in potential range from −1.2 to 0.2 V. Electrochemical impedance spectroscopy (EIS) was carried out with potentiostat/galvanostat/EIS (Biologic sp-150). The impedance spectra were measured by sweeping the frequency between the 1 MHz and 10 mHz in an oxygen-saturated 0.10 M KOH solution.

3. Results and discussion

3.1. Physical investigations of NG

3.1.1. SEM, TEM and XPS

The morphological features of synthesized NG were identified by SEM and TEM. Fig. 2(a) and (b) are SEM images of NG synthesized by solvothermal process. The sample contains a large number of nanoflower-like structures, each composed of many loose NG sheets. Fig. 2(c) and (d) show TEM images of the NG sheets. It can be observed that the graphene sheets have formed circular structures 100–200 nm in diameter.

XPS measurement was done to determine the content and features of nitrogen species. As shown in Fig. 2(e), three distinct peaks can be observed. The peaks at about 284.8, 399 and 534.5 eV denote the binding energy of C1s, N1s and O1s, respectively. The presence of an N1s peak around 400 eV indicates the successful incorporation of nitrogen atoms into the graphene sheets. The amount of nitrogen incorporated into the NG was about 4%.

The nature of the N functionalities in the resulting NG can be determined by the structure of the nitrogen source [13]. The nitrogen content and proportion of N species in the carbon materials can improve the activity of NG [14]. Previous studies have found that quaternary and pyridinic nitrogen are the most important

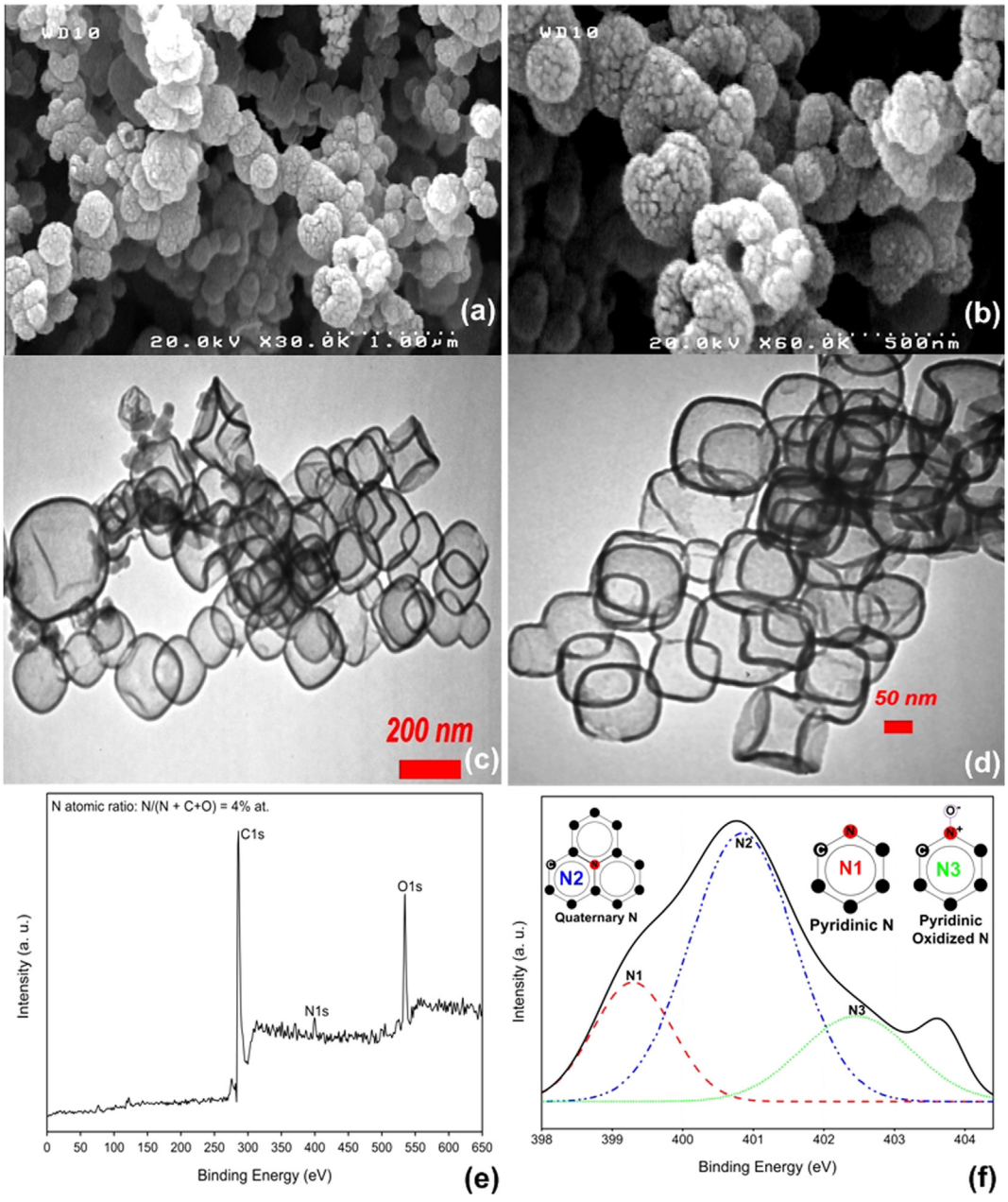

Fig. 2. (a, b) SEM images of synthesized NG; (c, d) TEM images of NG at different magnifications; (e) XPS spectrum of NG; (f) deconvoluted N1s region for NG.

species for catalyzing ORR due to the matching relationship between activity and nitrogen content [13,34]. The bonding configuration of carbon and nitrogen atoms of pentachloropyridine is shown in Fig. 1. It is evident that this component contains pyridinic nitrogen; it is thus expected that synthesized graphene will consequentially contain greater amounts of pyridinic nitrogen.

Fig. 2(f) shows a typical high-resolution N1s spectrum of NG. The types of nitrogen species were identified by curve-fitting. The complex N1s spectrum was further deconvoluted into three peaks at binding energies of 399.2, 400.9, and 402.5 eV, corresponding to pyridinic N, quaternary N and pyridine-N-oxide, respectively [35,47].

XPS analysis (Fig. 2(f)) of the N1s spectrum shows that only pyridinic-N, quaternary-N, and pyridine-N-oxide formed in the synthesized NG by the designed reaction. Recent studies have suggested that more active carbon catalysts might contain higher amounts of pyridinic and quaternary (graphitic) nitrogen [24,32]. Pyridinic N bonds with two C atoms at the edges or defects of the graphene and contributes one p electron to the π system (Fig. 2(f)). It has been shown that pyridinic N efficiently changes the valence band structure of graphene and one lone pair of electrons in pyridinic nitrogen facilitates reductive oxygen adsorption [35].

Quaternary-N is a type of nitrogen that bonds to three carbon atoms in the plane of the carbon matrix (Fig. 2(f)). O_2 molecules are

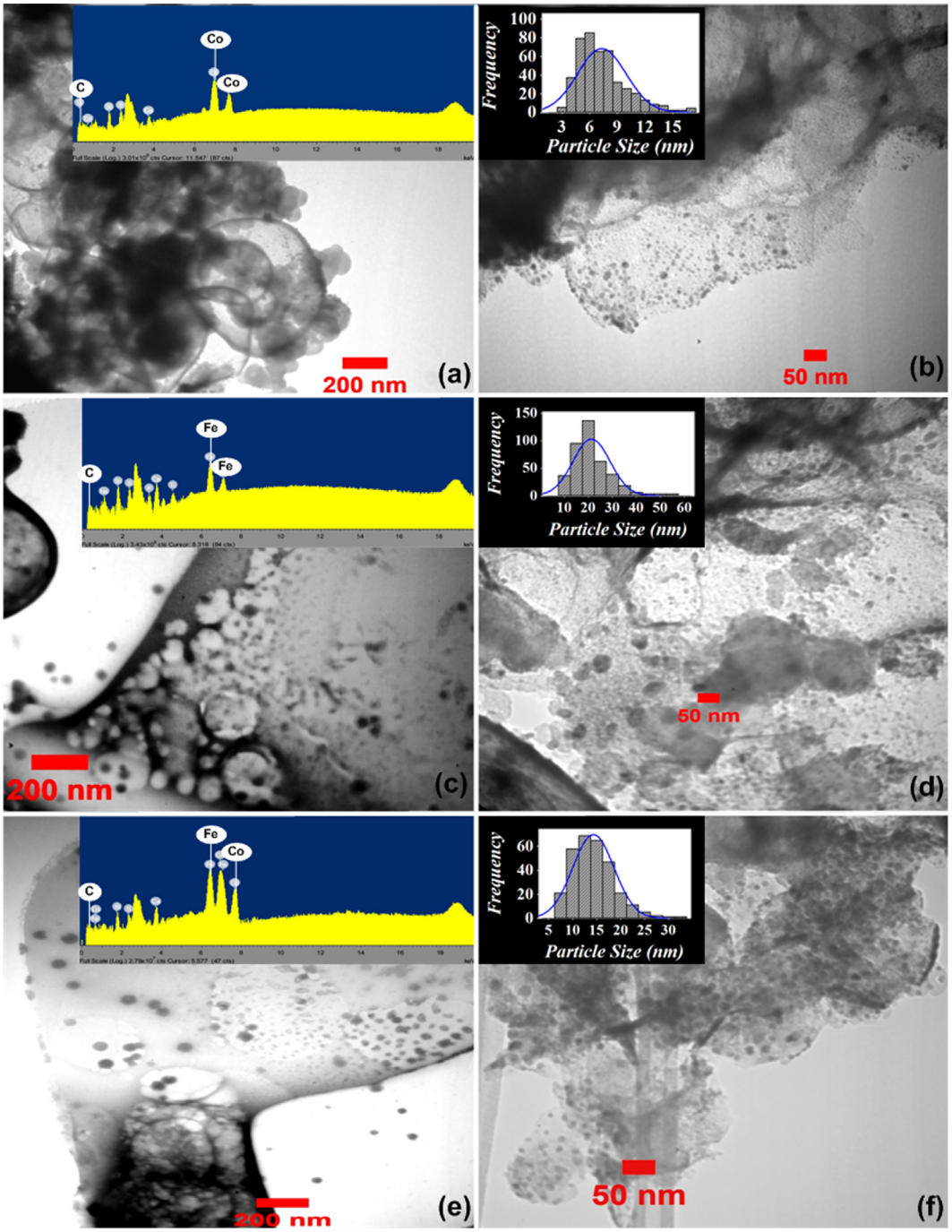

Fig. 3. (a) TEM image of Co/NG; (b) EDX image of Co/NG; (c) TEM image of Fe/NG; (d) EDX image of Fe/NG; (e) TEM image of Fe–Co/NG; (f) EDX image of Fe–Co/NG.

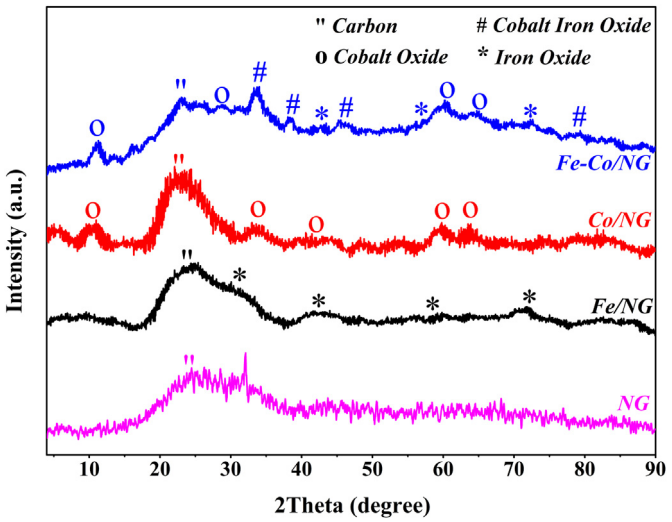

Fig. 4. XRD patterns for Fe–Co/NG, Co/NG and Fe/NG.

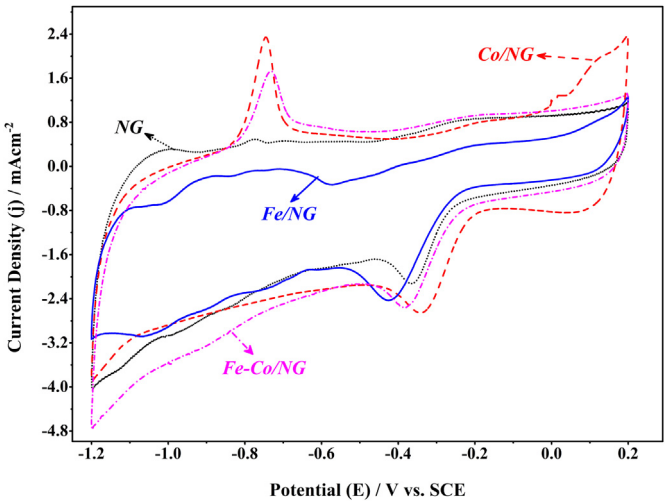

Fig. 6. CVs in O_2-saturated 0.1 M KOH solution for different electrodes at a scanning rate of 100 mV s^{-1}.

preferentially adsorbed at the carbon sites on the graphene-like zigzag edges if a quaternary-N is located nearby [32]. Previous research on nitrogen-modified carbon-based catalysts has shown that catalysts with a higher content of quaternary-N show higher ORR activity [13,27]. Based on this, the proposed NG is a promising support and electrocatalyst for ORR because this synthesized NG has a large amount of pyridinic and quaternary nitrogen. In this synthesis method [9], the precursor for both nitrogen and carbon was pentachloropyridine; as expected, the synthesized NG shows an ordered nanostructure and strong bonding between the nitrogen and carbon.

3.2. Physical characterization of M/NG catalysts

Fig. 3 provides TEM images showing the nanostructure of the M/NG catalysts. The metal nanoparticles are well-dispersed on the graphene sheets, demonstrating the formation of supported electrocatalysts. The small black spots on the graphene sheet are nanoparticles dispersed on the NG surface; the low degree of metal nanoparticles agglomeration results from the preparation process. Since ethylene glycol is a reducing, stabilizing and dispersing agent in the modified polyol reduction method, the distribution of metal nanoparticles was uniform and had a narrow size distribution. The nitrogen doping of the supporting material produced highly dispersed nanoparticles over the graphene support. The average size of the nanoparticles was 8.6 nm for Co/NG, 26.2 nm for Fe/NG, and 15.8 nm for Fe–Co/NG. The insets in Fig. 3(a), (c) and (e) presented EDX spectrum for the M/NG catalysts which demonstrated that Fe and Co were distributed on NG.

Fig. 4 shows the XRD patterns for Co/NG, Fe/NG, and Fe–Co/NG composites. All samples had broad peaks (2θ: 18–32°) corresponding to the graphene plane diffraction (002) [48]. The average crystallite sizes calculated using Scherer's equation were 10.1 nm for Co/NG, 26 nm for Fe/NG, and 17.6 nm for Fe–Co/NG. These results were in good agreement with previous TEM data.

3.3. Electrochemical characterization

3.3.1. Cyclic voltammetry (CV) and linear sweep voltammetry (LSV)

The electrocatalytic activity of the synthesized NG was determined using a conventional three-electrode system in an alkaline solution. Fig. 5(a) shows a clean capacitive CV background in

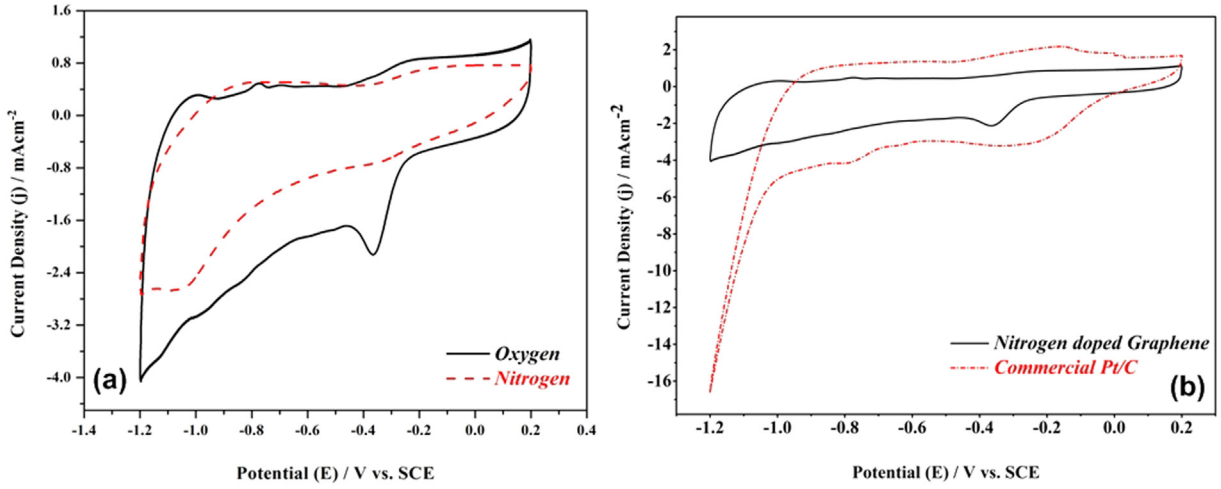

Fig. 5. Electrocatalytic activity of NG for ORR (a) CV curves of NG in nitrogen or oxygen saturated 0.1 M KOH at a scanning rate of 100 mV s^{-1}; (b) CV curves of NG and commercial Pt/C electrode in 0.1 M KOH at a scanning rate of 100 mV s^{-1}.

nitrogen-saturated 0.1 M KOH solution. In the presence of oxygen, a prominent cathodic current appeared with a peak centered at ~−0.35 V vs. SCE and specifies the pronounced electrocatalytic activity of synthesized NG alone for ORR.

Cyclic voltammograms of the synthesized NG and commercial Pt/C (40%; Sigma Aldrich) are shown in Fig. 5(b). The existence of a cathodic peak with a current density of −2.13 mA cm^{-2} shows that NG alone shows acceptable activity for ORR in an alkaline media. This can be attributed to the presence of pyridinic and graphitic (quaternary) nitrogen types in the graphene matrix; these types of nitrogen play an important role in electrocatalysis for ORR. Pyridinic nitrogen creates a higher proportion of edge planes and structural defects on graphene that actively react with oxygen and form oxygen-containing groups when exposed to air [34,49,50].

A further increase in activity is required to allow NG to compete with commercial platinum catalyst, so iron and cobalt nanoparticles were deposited on synthesized NG as a supporting material in next step. The CV curves for the NG, Fe/NG, Co/NG and Fe–Co/NG catalysts are shown in Fig. 6. The CV diagrams of catalysts with metal nanoparticles show more positive ORR peak potentials. It is also evident from a comparison of the CV curves that Co/NG is the most active catalyst with more positive peak potential (−0.33 V). This improvement in electrocatalytic activity can be attributed to the presence of more electroactive sites after the precipitation of Fe and Co nanoparticles than for the NG electrode.

The particle size distribution shown in the TEM and XRD data indicate that the Co/NG sample showed smaller nanoparticles and better dispersion than the Fe–Co/NG and Fe/NG samples. The better dispersion of cobalt nanoparticles facilitated adsorption of oxygen molecules and these active sites promote ORR better than do the other electrocatalysts.

Fig. 7 shows the electrocatalytic performance of Co/NG compared to commercial Pt/C. The prominent reduction peak at −0.33 V in alkaline solution suggests increased electrocatalytic activity of Co/NG for ORR. It is clear from the cyclic voltammetry diagram that peak potential of Pt/C catalyst is in the range of ~−0.12 to ~−0.24 V and the peak potential of Co/NG is −0.33 V which shows promising activity of Co/NG catalyst for ORR.

The oxygen reduction activities of non-precious metal-based catalysts were further investigated using LSV. Fig. 8(a) shows a series of LSV curves for different catalysts measured in O_2-saturated 0.1 M KOH at a sweep rate of 10 mV s^{-1}. A comparison of these catalysts indicates that, relative to Fe/NG and Fe–Co/NG, Co/NG showed higher activity. This is evidenced by the 64 mV positive shift at onset from −0.203 to −0.1398 V for Fe/NG and 21 mV from −0.1609 to −0.1398 V for Fe–Co/NG and the 60 mV positive shift in half-wave (E1/2) from −0.2602 to −0.2 V for Fe/NG and 54 mV from −0.2541 to −0.2 V for Fe–Co/NG sample. The significant improvement in ORR performance for Co/NG catalyst is in agreement with the CV results. This increased electrocatalytic activity of Co/NG could be the result of the smaller size distribution of cobalt nanoparticles on the NG sheets.

Co/NG showed the best performance and its LSV curve is compared with those for NG alone and commercial platinum in Fig. 8(b). It is clear that the absolute value of reduction current density for Co/NG improved from −0.48 to −01.34 mA cm^{-2} and the onset potential exhibited 81 mV positive shift compared with NG alone (from −0.2211 to −0.1398 V). A comparison of Pt/C catalyst and Co/NG showed about a 26% decrease in reduction current density (−1.34 mA cm^{-2} for Co/NG, −1.83 mA cm^{-2} for Pt/C). The performance of Co/NG was much lower than for Pt/C in terms of onset potential and half-wave potential.

Fig. 8(a) and (b) show a general increase in the activity of synthesized catalysts for ORR after metal precipitation. Although ORR

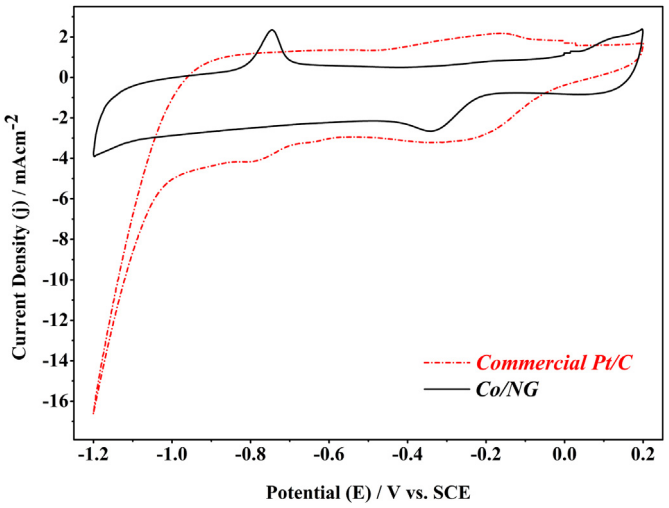

Fig. 7. CVs in O_2-saturated 0.1 M KOH solution for Co/NG and commercial Pt/C at a scanning rate of 100 mV s^{-1}.

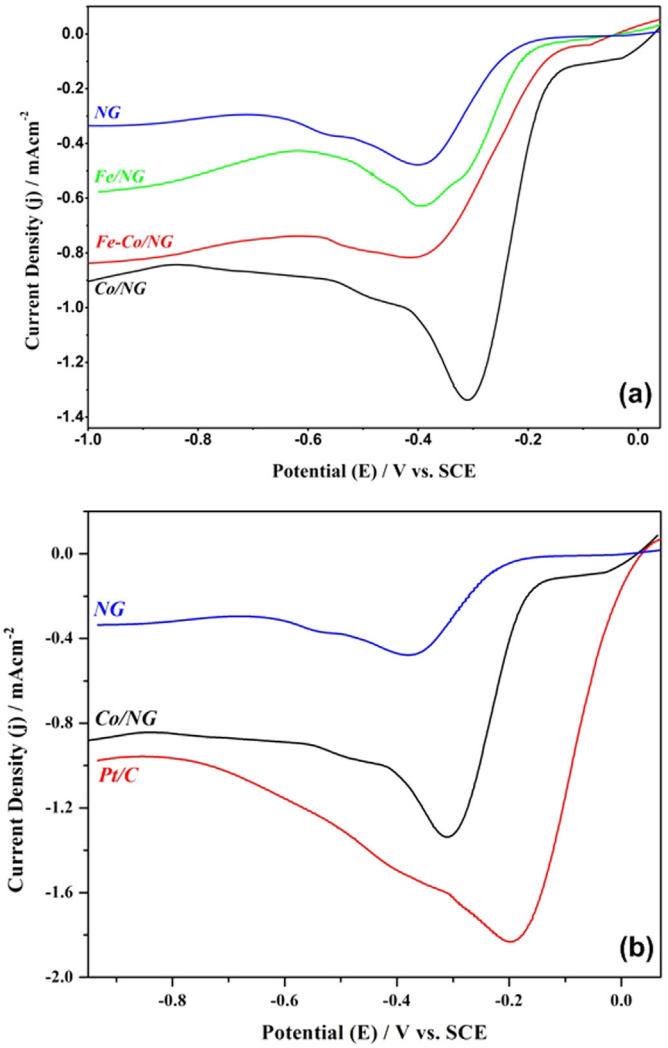

Fig. 8. (a) LSVs for NG, Fe/NG, Fe–Co/NG, and Co/NG electrodes in O_2-saturated 0.1 M KOH solution at a scanning rate of 10 mV s^{-1}; (b) LSVs for ORR obtained at Co/NG, NG alone and commercial Pt/C electrodes at a scanning rate of 10 mV s^{-1}.

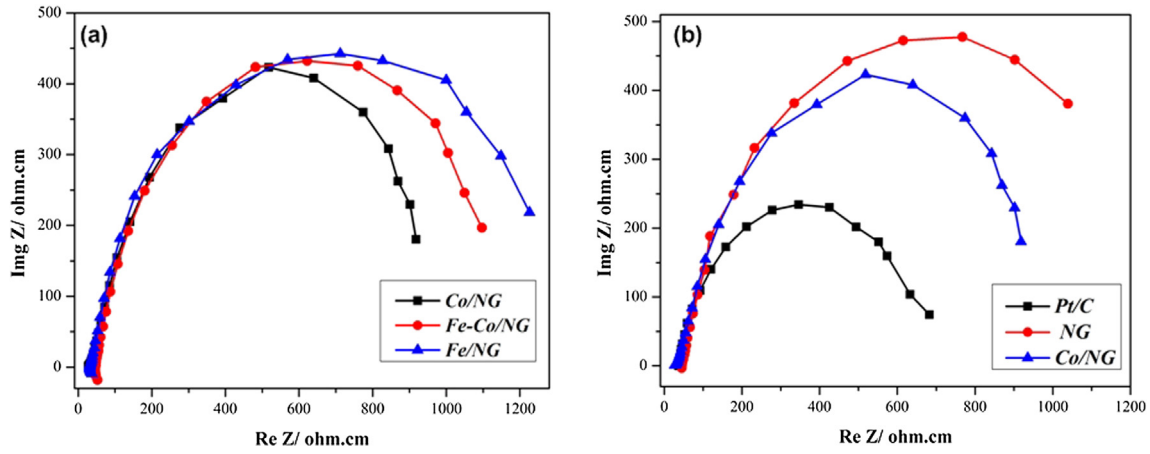

Fig. 9. Nyquist diagrams of (a) Fe/NG, Fe–Co/NG, Co/NG; (b) Co/NG, NG alone, and commercial Pt/C at −250 mV in O_2 saturated 0.1 M KOH solution.

activity did not dramatically increase, the half-wave potentials and reduction current densities moved closer to those of Pt/C. This shows that transitional metal nanoparticles supported on NG material took part in ORR and increased the activity of NG for ORR. These transitional metal nanoparticles can be considered to be electroactive sites for ORR. The optimal dispersion of metal nanoparticles on NG materials may increase the activity of the final catalyst because it exposes more active sites to the reactants.

TEM results shown in Section 3.2 confirm that the Co/NG sample showed more uniform dispersion of metal nanoparticles and smaller particle size than the Fe/NG and Fe–Co/NG samples, meaning that the Co/NG catalyst had a higher electroactive surface area and good accessibility of metal sites for oxygen adsorption. As reported in previous studies [44,45], the modified polyol reduction approach yields uniform dispersion, higher loading and optimum particle size of catalyst nanoparticles over supporting materials than the conventional sodium borohydride reduction method.

3.3.2. *Electrochemical impedance spectroscopy*

The electron transfer kinetics of ORR in the modified electrodes was studied using selected EIS measurements. EIS is a powerful technique that enables evaluation of physical and interfacial properties of modified electrodes. The charge-transfer resistance corresponds to the diameter of a semicircle on the Nyquist impedance plot. The Nyquist diagrams for Fe/NG, Co/NG and Fe–Co/NG electrodes were recorded at −250 mV vs. SCE. EIS measurements in Fig. 9(a) show the diameter of the impedance arc for Co/NG electrocatalyst is smaller than those for Fe/NG and Fe–Co/NG for applied potential, indicating increased kinetics for O_{ads} chemisorption and ORR. These results suggest faster electron transfer kinetics and, consequently, better electrocatalytic performance for the Co/NG catalyst when compared with Fe/NG and Fe–Co/NG catalysts, which is in good agreement with the results of the ORR measurements.

Fig. 9(b) compares the EIS behavior of NG, Co/NG and commercial Pt/C electrodes. It is clear from the Nyquist diagrams that Co/NG catalyst shows increased electrocatalytic performance, because the diameter of its impedance arc is smaller than that of the NG alone. This suggests that the charge-transfer reactions have become faster, but the kinetics are still weaker than for Pt/C.

The stability of Co/NG and commercial Pt/C catalysts was tested at a constant voltage of −0.25 V (vs. SCE) for 15,000 s in oxygen-saturated 0.1 M KOH. As shown in Fig. 10, the chronoamperometric response for Co/NG catalyst exhibited slow attenuation with relatively high current retention. Continuous oxygen reduction on the Co/NG electrode resulted in about a 10% loss in current compared to the 40% loss for Pt/C electrode under the same testing conditions. These results indicate that active sites on the Co/NG electrode are more stable than those on commercial Pt/C electrode. The better stability of the Co/NG catalyst can be attributed to strong covalent bonds between the active sites and graphitic lattice and to

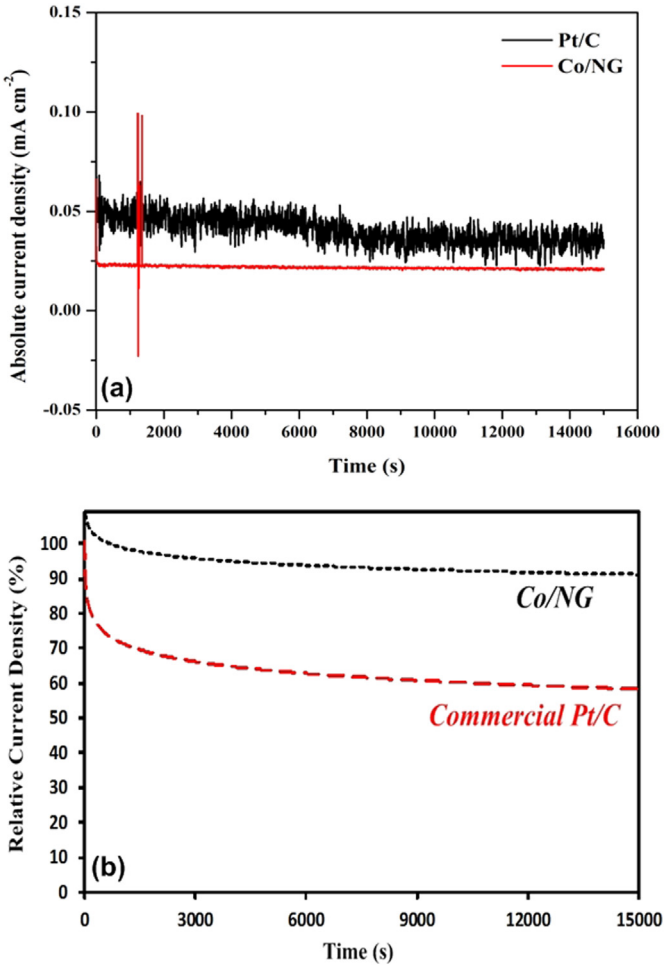

Fig. 10. Chronoamperometric responses for ORR for Co–N–GN and Pt/C catalysts in O_2-saturated 0.1 M KOH solution at −0.3 V vs. SCE.

the presence of nitrogen atoms that create anchoring sites for metal nanoparticle deposition and enhance their stability on the graphene sheets. The basal plane of graphene prevents metal nanoparticle agglomeration during fuel cell performance and increases the durability of catalyst for electrochemical reactions, making it a promising catalyst for alkaline fuel cells.

4. Conclusion

Simple approaches were explored for synthesis of NG-supported non-precious catalysts for ORR in alkaline media. It was observed that metal nanoparticles and nitrogen species significantly increased ORR electrocatalytic activity in M/NG catalysts. Co/NG catalyst presented higher reduction current density and an 81 mV positive shift in onset potential in comparison with NG alone in alkaline solution. This indicates that transitional metal nanoparticles can act as electroactive sites for ORR.

The electrocatalytic properties of M/NG electrodes were closely related to the particle size distribution in the order of Co/NG > Fe–Co/NG > Fe/NG. Importantly, Co/NG also exhibited excellent stability compared with commercial Pt/C for ORR in alkaline media. Although the activity of the synthesized catalysts was weaker than for commercial platinum, a change in metal loading and improvement in the structure of graphene can further increase catalyst activity.

This study demonstrates that M/NG catalysts are capable of replacing the more costly Pt/C for catalyzing ORR in fuel cells. This approach may open new avenues for producing non-precious, active and durable electrocatalysts with simple process stages for oxygen reduction reaction.

References

[1] S. Guo, S. Sun, J. Am. Chem. Soc. 134 (2012) 2492–2495.
[2] V. Neburchilov, H. Wang, J.J. Martin, W. Qu, J. Power Sources 195 (2010) 1271–1291.
[3] S. Zhang, Y. Shao, G. Yin, Y. Lin, J. Mater. Chem. 19 (2009) 7995–8001.
[4] Y. Shao, G. Yin, Y. Gao, J. Power Sources 171 (2007) 558–566.
[5] M. Watanabe, D.A. Tryk, M. Wakisaka, H. Yano, H. Uchida, Electrochim. Acta 84 (2012) 187–201.
[6] E. Antolini, Appl. Catal. B Environ. 74 (2007) 337–350.
[7] V. Bambagioni, C. Bianchini, J. Filippi, A. Lavacchi, W. Oberhauser, A. Marchionni, S. Moneti, F. Vizza, R. Psaro, V. Dal Santo, A. Gallo, S. Recchia, L. Sordelli, J. Power Sources 196 (2011) 2519–2529.
[8] K.-W. Nam, J. Song, K.-H. Oh, M.-J. Choo, H. Park, J.-K. Park, J.W. Choi, Carbon 50 (2012) 3739–3747.
[9] D. Geng, Y. Hu, Y. Li, R. Li, X. Sun, Electrochem. Commun. 22 (2012) 65–68.
[10] Z. Mo, S. Liao, Y. Zheng, Z. Fu, Carbon 50 (2012) 2620–2627.
[11] S. Shanmugam, T. Osaka, Chem. Commun. 47 (2011) 4463–4465.
[12] W. Shen, W. Fan, J. Mater. Chem. A 1 (2013) 999–1013.
[13] Z. Lin, G.H. Waller, Y. Liu, M. Liu, C.-p. Wong, Carbon 53 (2013) 130–136.
[14] J. Wu, D. Zhang, Y. Wang, B. Hou, J. Power Sources 227 (2013) 185–190.
[15] H. Li, H. Liu, Z. Jong, W. Qu, D. Geng, X. Sun, H. Wang, Int. J. Hydrogen Energy 36 (2011) 2258–2265.
[16] C. He, Z. Li, M. Cai, M. Cai, J.-Q. Wang, Z. Tian, X. Zhang, P.K. Shen, J. Mater. Chem. A 1 (2013) 1401–1406.
[17] D. Geng, Y. Chen, Y. Chen, Y. Li, R. Li, X. Sun, S. Ye, S. Knights, Energy Environ. Sci. 4 (2011) 760–764.
[18] B. Xiong, Y. Zhou, Y. Zhao, J. Wang, X. Chen, R. O'Hayre, Z. Shao, Carbon 52 (2013) 181–192.
[19] R. Imran Jafri, N. Rajalakshmi, S. Ramaprabhu, J. Mater. Chem. 20 (2010) 7114–7117.
[20] S. Maldonado, K.J. Stevenson, J. Phys. Chem. B 108 (2004) 11375–11383.
[21] S. Maldonado, K.J. Stevenson, J. Phys. Chem. B 109 (2005) 4707–4716.
[22] V. Nallathambi, J.-W. Lee, S.P. Kumaraguru, G. Wu, B.N. Popov, J. Power Sources 183 (2008) 34–42.
[23] A. Zahoor, M. Christy, Y.J. Hwang, Y.R. Lim, P. Kim, K.S. Nahm, Appl. Catal. B Environ. 147 (2014) 633–641.
[24] Z.-J. Lu, S.-J. Bao, Y.-T. Gou, C.-J. Cai, C.-C. Ji, M.-W. Xu, J. Song, R. Wang, RSC Adv. 3 (2013) 3990–3995.
[25] C. Huang, C. Li, G. Shi, Energy Environ. Sci. 5 (2012) 8848–8868.
[26] L.-S. Zhang, X.-Q. Liang, W.-G. Song, Z.-Y. Wu, Phys. Chem. Chem. Phys. 12 (2010) 12055–12059.
[27] B. Zheng, J. Wang, F.-B. Wang, X.-H. Xia, Electrochem. Commun. 28 (2013) 24–26.
[28] B.F. Machado, P. Serp, Catal. Sci. Technol. 2 (2012) 54–75.
[29] Y. Shao, J. Sui, G. Yin, Y. Gao, Appl. Catal. B Environ. 79 (2008) 89–99.
[30] Z. Mou, X. Chen, Y. Du, X. Wang, P. Yang, S. Wang, Appl. Surf. Sci. 258 (2011) 1704–1710.
[31] Y. Shao, S. Zhang, M.H. Engelhard, G. Li, G. Shao, Y. Wang, J. Liu, I.A. Aksay, Y. Lin, J. Mater. Chem. 20 (2010) 7491–7496.
[32] G. Liu, X. Li, J.-W. Lee, B.N. Popov, Catal. Sci. Technol. 1 (2011) 207–217.
[33] Q. Liu, H. Zhang, H. Zhong, S. Zhang, S. Chen, Electrochim. Acta 81 (2012) 313–320.
[34] N.P. Subramanian, X. Li, V. Nallathambi, S.P. Kumaraguru, H. Colon-Mercado, G. Wu, J.-W. Lee, B.N. Popov, J. Power Sources 188 (2009) 38–44.
[35] Z. Luo, S. Lim, Z. Tian, J. Shang, L. Lai, B. MacDonald, C. Fu, Z. Shen, T. Yu, J. Lin, J. Mater. Chem. 21 (2011) 8038–8044.
[36] D. Wei, Y. Liu, Y. Wang, H. Zhang, L. Huang, G. Yu, Nano Lett. 9 (2009) 1752–1758.
[37] C.W.B. Bezerra, L. Zhang, K. Lee, H. Liu, A.L.B. Marques, E.P. Marques, H. Wang, J. Zhang, Electrochim. Acta 53 (2008) 4937–4951.
[38] X. Li, G. Liu, B.N. Popov, J. Power Sources 195 (2010) 6373–6378.
[39] X. Li, B.N. Popov, T. Kawahara, H. Yanagi, J. Power Sources 196 (2011) 1717–1722.
[40] S.H. Lim, Z. Li, C.K. Poh, L. Lai, J. Lin, J. Power Sources 214 (2012) 15–20.
[41] X. Fu, Y. Liu, X. Cao, J. Jin, Q. Liu, J. Zhang, Appl. Catal. B Environ. 130–131 (2013) 143–151.
[42] G. Wu, M. Nelson, S. Ma, H. Meng, G. Cui, P.K. Shen, Carbon 49 (2011) 3972–3982.
[43] K. Kamiya, K. Hashimoto, S. Nakanishi, Chem. Commun. 48 (2012) 10213–10215.
[44] B.P. Vinayan, R.I. Jafri, R. Nagar, N. Rajalakshmi, K. Sethupathi, S. Ramaprabhu, Int. J. Hydrogen Energy 37 (2012) 412–421.
[45] D.-S. Yang, M.-S. Kim, M.Y. Song, J.-S. Yu, Int. J. Hydrogen Energy 37 (2012) 13681–13688.
[46] B.P. Vinayan, K. Sethupathi, S. Ramaprabhu, Int. J. Hydrogen Energy 38 (2013) 2240–2250.
[47] K.R. Lee, K.U. Lee, J.W. Lee, B.T. Ahn, S.I. Woo, Electrochem. Commun. 12 (2010) 1052–1055.
[48] S.-K. Park, A. Jin, S.-H. Yu, J. Ha, B. Jang, S. Bong, S. Woo, Y.-E. Sung, Y. Piao, Electrochim. Acta 120 (2014) 452–459.
[49] P.H. Matter, L. Zhang, U.S. Ozkan, J. Catal. 239 (2006) 83–96.
[50] A. Montoya, F. Mondragón, T.N. Truong, Fuel Process. Technol. 77–78 (2002) 453–458.